Kovove Mater. 63 2025 107–117
DOI: 10.31577/km.2025.2.107

A comparative study of Fm-3m TiO_2, ZrO_2, HfO_2, and CeO_2 via atomistic modeling

Farouk Mebtouche[1], Saddik Elhak Abaidia[1], Bachireddine Messaid[2], Younes Lamri[2], Nadia Nehaoua[1]

[1] *Laboratory of Coatings, Materials, and Environment (LRME), University of Boumerdes (UMBB), 35000, Boumerdes, Algeria*
[2] *Research Unit, Materials, Processes and Environment (URMPE), University of Boumerdes (UMBB), 35000, Boumerdes, Algeria*

Received 23 January 2025, received in revised form 19 February 2025, accepted 28 April 2025

Abstract

Metal oxides (XO_2) have been extensively studied experimentally and theoretically. However, atomistic insights into systems like ZrO_2 and CeO_2, critical in nanocatalysis, remain incomplete. Using ab initio density functional theory (DFT) with the FP-LAPW method in the Wien2k framework and the PBE exchange-correlation functional, we examined the physical and chemical properties of cubic Fm-3m oxides (XO_2, X = Ti, Zr, Hf, Ce). Lattice parameters increase with atomic mass except for HfO_2, which deviates due to stronger ionic bonding. ZrO_2 is the stiffest, followed by HfO_2, TiO_2, and CeO_2. Electronic analysis shows TiO_2's narrow band gap (1.15 eV), ZrO_2 and HfO_2's wide gaps (3.16 and 3.77 eV), and CeO_2's moderate gap (2.17 eV) with redox activity. PDOS analysis highlights O 2p and metal d-/f-orbital interactions. These results emphasize distinct properties influencing their applications in photocatalysis, dielectrics, and catalysis, warranting further exploration.

K e y w o r d s: Ab initio, oxides, stiff, band gap, orbitals

1. Introduction

Metal oxides are an essential class of materials known for their diverse properties and widespread applications in various technological and industrial fields. Those with moderate to wide band gaps, such as TiO_2, ZrO_2, HfO_2, and CeO_2 are particularly notable for their roles in semiconductors for dye-sensitized solar cells, catalysts, fuel cells, resistors, gas sensors, transparent optical devices, and optical coatings [1–7]. Their unique characteristics, such as chemical stability, optical transparency, and tunable electronic properties, make them highly versatile. The functional performance of these oxides is influenced by several factors, including particle size, crystallinity, surface area, and synthesis techniques, which play critical roles in determining their structural, electronic, and surface properties [8–11].

TiO_2 is widely recognized for its applications in photocatalysis, solar energy devices, and environmental remediation [12–22]. It has various structural forms, including rutile, anatase, brookite, and cubic Fm-3m phases [23, 24]. While the rutile and anatase phases are naturally stable and commonly employed in practical applications, the cubic Fm-3m phase structure (Fig. 1) is metastable and typically synthesized under high-pressure or specific deposition conditions [25, 26]. This cubic form offers unique properties, such as enhanced optical and electronic behavior, which make it promising for advanced technologies.

ZrO_2, on the other hand, is renowned for its exceptional thermal and mechanical properties, making it indispensable in applications such as thermal barrier coatings and solid oxide fuel cells [27–33]. While the material naturally adopts a monoclinic configuration at standard conditions, it can be transformed into a cubic Fm-3m structure through thermal treatment or by introducing specific dopants like yttria or rare-earth elements. The resulting phase transforma-

*Corresponding author: e-mail address: f.mebtouche@univ-boumerdes.dz

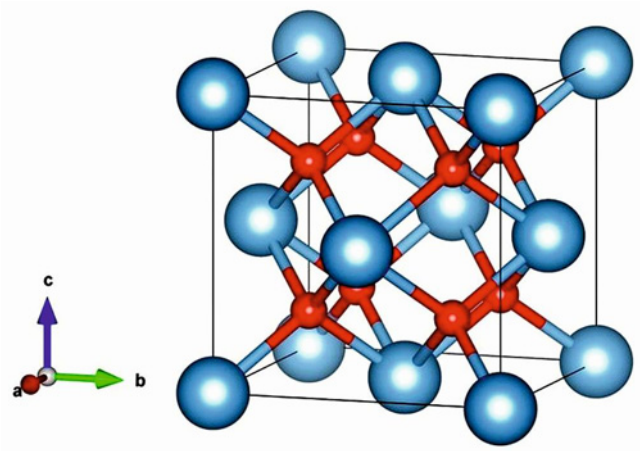

Fig. 1. Fm-3m phase structure (Ti, Zr, Hf, Ce in Cyan): at (0, 0, 0), (1/2, 1/2, 1/2), (1/2,0,0), (0,1/2,0), (0,0,1/2); oxygen o in red at: (1/4, 1/4, 1/4), (3/4, 3/4, 3/4).

tion dramatically improves the material's ability to conduct ions, making it particularly valuable for advanced energy applications [34–44]. Its robust nature and ability to withstand extreme conditions make it suitable for structural ceramics and high-temperature applications.

On the other hand, HfO_2 shares many similarities with ZrO_2 but stands out due to its exceptional dielectric properties, which have positioned it as a cornerstone material in modern microelectronics, particularly as a high-k dielectric in semiconductor devices [45–49]. Like ZrO_2, HfO_2 exists in monoclinic, tetragonal, and cubic phases, with the cubic Fm-3m phase stabilized at elevated temperatures or under specific doping conditions [50, 51]. This phase provides enhanced thermal stability and mechanical robustness, making HfO_2 suitable for demanding applications, including aerospace technologies and thermal barrier coatings. Its ability to maintain structural and electronic integrity under extreme conditions further highlights its potential in advanced technological applications.

Furthermore, CeO_2, similar to the other oxides discussed, is a highly versatile material with significant applications in catalysis, energy storage, and environmental remediation [52–55]. Its most stable phase at ambient conditions is the cubic Fm-3m fluorite structure, which is crucial for its remarkable catalytic properties [56, 57]. The Fm-3m phase facilitates efficient oxygen vacancy migration, a key feature that drives CeO_2's redox activity and enables its vital role in automotive catalytic converters and fuel cells [58, 59]. Beyond catalysis, CeO_2's stability, high ionic conductivity, and ability to operate under extreme conditions make it indispensable in energy storage systems and other advanced technologies [60]. These characteristics, along with its durability and structural integrity, reinforce CeO_2's potential in cutting-edge applications.

Although numerous studies have explored the properties of TiO_2, ZrO_2, HfO_2, and CeO_2, both experimentally and theoretically [61–65], there remains a notable gap in the literature regarding the understanding of the differences between these oxides, especially when considering them in the same phase structure, such as the cubic Fm-3m phase. These oxides, which belong to Group 4 and Group 5 of the periodic table, share similar chemical families but may exhibit distinct structural, mechanical, and electronic properties. This study aims to address this gap by systematically investigating whether intrinsic differences exist in the properties of these oxides under identical structural conditions, shedding light on their unique characteristics and providing deeper insights into their potential applications.

The content of this study is arranged in the following sequence: in section 2, we provide a thorough explanation of the computational procedures, parameters, and setup utilized throughout this investigation. The third section presents the results and discussion, focusing on the structural, mechanical, and electronic properties of the cubic oxides (c-TiO_2, c-ZrO_2, c-HfO_2, and c-CeO_2). Finally, the article summarizes the key findings and insights from this comparative study.

2. Computational details

The structural, elastic, and electronic properties of the TMs Fm-3m XO_2 (X = Ti, Zr, Hf, Ce) oxides were studied using the full-potential linearized augmented plane wave (FP-LAPW) method [66, 67]. The Kohn–Sham equations [68] were solved within the density functional theory framework. The calculations employed the generalized gradient approximation (GGA). In the full-potential scheme, the wave function, potential, and charge density are expanded into two separate bases [69]. Inside the atomic spheres, the wave function is expanded in spherical harmonics, while in the interstitial regions, it is represented using plane waves. The muffin-tin radii (RMT) were chosen to prevent charge leakage from the core and to ensure better energy eigenvalue convergence. The RMT values were set to 2.0 a.u. for Ti, Zr, and Hf, 2.22 a.u. for Ce, and 1.75 a.u. for O. The plane-wave expansion was truncated at $Rk_{\max} = 8.0$, ensuring a well-converged basis set while maintaining computational efficiency. The self-consistency criterion for total energy convergence was set to 10^{-6} Ry.

The wave functions in the interstitial region were expanded in plane waves with a cutoff of 75 Ry. Integrals over the Brillouin zone were performed using 216 k-points for GGA Perdew-Burke-Ernzerhof (PBE)

Table 1. Lattice parameters and bulk modulus of various cubic oxides

Oxides	a_0 (Å)	B (GPa)	B'	Reference
c-TiO_2	4.836	293.75	4.375	This work
	4.73	286	3.99	Ref. [73]
	4.87	202	1.3	Exp. [74]
c-ZrO_2	5.15	233.44	4.26	This work
	5.151	228	4.43	Ref. [87]
	5.11	–	–	Exp. [88]
c-HfO_2	5.102	248.327	4.272	This work
	5.071	–	–	Ref. [87]
	5.08	–	–	Exp. [76]
c-CeO_2	5.473	142.85	4.049	This work
	5.44	184.9	4.24	Ref. [75]
	5.41	204	4.4	Exp. [77]

[70] in the irreducible Brillouin zone, with the modified tetrahedron method [71]. For electronic properties, a dense mesh of k-points was used. The Brillouin zone integration was carried out with 1728 k-points in PBE.

3. Results and discussion

3.1. Structural properties

The structural properties of XO_2 (X = Ti, Zr, Hf, Ce) are obtained by fitting the total energy of each unit cell against its volume using the Birch-Murnaghan equation of state [72]. The unit cell volume of the compounds is optimized to obtain structural properties like lattice constant, a_0 (Å), bulk moduli B (GPa), and the bulk modulus derivative B'. The calculated structural parameters are presented in Table 1.

TiO_2: The lattice parameter a_0, bulk modulus B, and pressure derivative B' of TiO_2 vary across different studies, reflecting differences in computational and experimental approaches. The obtained value of a_0 (4.836 Å) lies between those found in other references, 4.73 Å [73] and 4.87 Å [74], with the larger a_0 in the experimental value [74] suggesting that real-world factors, such as thermal expansion and imperfections, contribute to the variation. The bulk modulus B in this work (293.75 GPa) is higher than both the theoretical value (286 GPa) and the experimental value (202 GPa), indicating that theoretical models predict a stiffer material, possibly due to idealized conditions, while experimental values are influenced by defects and temperature effects. Similarly, the pressure derivative B' in this work (4.375) is higher than the theoretical value (3.99) and much larger than the experimental value (1.3), suggesting that theoretical models predict a stronger increase in incompressibility under pressure than observed experimentally. However, despite these small differences, our results are in good agreement with both previous DFT calculations and experimental reports.

ZrO_2: The calculated structural properties of c-ZrO_2 show a good agreement across various studies. The lattice parameter a_0 is 5.15 Å. This value closely matches the one from the previous DFT finding (5.151 Å) and is slightly larger than the experimental value from (5.11 Å). The bulk modulus B in this work is 233.44 GPa. This value is slightly higher than the one in the DFT calculation (228 GPa), suggesting that the material is modeled as more incompressible under ideal conditions. The pressure derivative B' in this work is 4.26. This is somewhat lower than the value in [63] (4.43 Å), indicating a less pronounced increase in incompressibility with pressure compared to the theoretical prediction.

HfO_2: The obtained lattice parameter value a_0 is 5.102 Å, slightly larger than the value in [75] (5.071 Å) and similar to [76] (5.08 Å). The bulk modulus B is 248.327 GPa, but no data is available in the other references for comparison. The pressure derivative B' is 4.272, with no corresponding values in the other studies. Overall, our results are consistent with previous DFT and experimental findings.

CeO_2: In this work, a_0 is 5.473 Å, slightly larger than the values in [75] (5.44 Å) and [79] (5.41 Å). The bulk modulus B is 142.85 GPa, which is lower than the values in [75] (184.9 GPa) and [77] (204 GPa). The pressure derivative B' is 4.049, slightly smaller than both the values in the literature. Overall, the results are in good agreement with both DFT and experimental studies, showing only minor variations.

It is interesting to observe that the lattice parameters for TiO_2, ZrO_2, and CeO_2 increase with atomic mass, as expected due to the larger ionic radii of the

Table 2. The calculated elastic constants C_{11}, C_{12}, and C_{44}, bulk modulus B, Young's modulus E, shear modulus G

Oxides	C_{11}	C_{12}	C_{44}	B (GPa)	G (GPa)	E (GPa)	Reference
c-TiO_2	604.90	69.209	43.58	248.10	88.37	78.99	This work
	589	75	43	250	84	75.53	Ref. [79]
	603	75	43	251	90	80.39	Exp. [80]
c-ZrO_2	535	97	51	243.00	219.00	219.79	This work
	507	99	63	235	204.00	234.18	Ref. [81]
	596.33	137.04	74.34	290.134	136.464	545.12	Exp. [82]
c-HfO_2	564.08	86.71	94.90	245.83	127.27	102.24	This work
	559	93	69	248	115	99.6	Ref. [83]
	578.2	120.9	82.6	283.2	130	139.4	Exp. [84]
c-CeO_2	335	97	51	176.33	119	248.24	This work
	371.83	114.69	62.71	200.40	128.57	252.88	Ref. [85]
	354.790	139.272	51.195	211.11	107.76	255.28	Exp. [86]

metal cations in these compounds. However, the case of HfO_2 deviates from this pattern, with its lattice parameter being slightly smaller despite Hf having a higher atomic mass. This could be explained by stronger ionic bonding in HfO_2, which might counteract the expected increase in lattice size. The size of the Hf cation and factors like crystal packing, polarization effects, and electron shielding may lead to a more compact structure. Additionally, phase stability differences might also influence the lattice parameter of HfO_2.

The differences in bulk modulus for TiO_2, ZrO_2, HfO_2, and CeO_2 reflect bonding strength and crystal structure variations. TiO_2 has the highest bulk modulus (293.75 GPa), indicating it is the stiffest due to strong Ti-O bonds. ZrO_2 (233.44 GPa) and HfO_2 (248.33 GPa) show intermediate values, with HfO_2 slightly stiffer, possibly due to stronger Hf-O bonds. CeO_2 has the lowest bulk modulus (142.85 GPa), suggesting weaker Ce-O bonds and a more compressible structure.

The variations in the pressure derivative of the bulk modulus B' across TiO_2, ZrO_2, HfO_2, and CeO_2 show differences in how these materials respond to pressure. TiO_2 has the highest B' (4.375), indicating a greater increase in resistance to compression with pressure. ZrO_2 (4.26) and HfO_2 (4.272) show similar behavior, with moderate responses to pressure. CeO_2 has the lowest B' (4.049), suggesting a weaker increase in incompressibility under pressure. These differences imply that atomic size influences B', but bonding strength and structural characteristics mainly determine the pressure response.

3.2. Elastic properties

The elastic constants C_{ij} are used to characterize the material's response to applied macroscopic stress, providing valuable information on its stability and stiffness [67]. The values of C_{11}, C_{12}, and C_{44} are presented in Table 2. A crystal structure can only exist in a stable or metastable phase if its elastic constants satisfy specific relationships. The traditional mechanical stability conditions for cubic crystals at equilibrium are expressed in terms of elastic constants as described in Ref. [78]:

$$\begin{aligned} &C_{11} - C_{12} > 0, \\ &C_{44} > 0, \\ &C_{11} + 2C_{12} > 0. \end{aligned} \tag{1}$$

3.2.1. Elastic constants

The present table compares the elastic constants and mechanical properties of c-TiO_2. The properties include C_{11}, C_{12}, C_{44}, bulk modulus (B), shear modulus (G), and Young's modulus (E). This work reports C_{11} as 604.90 GPa, which is slightly higher than 589 GPa in [79] and similar to 603 GPa in [82].

This indicates a higher resistance to uniaxial compression in this work compared to [79], with consistency observed between this work and [80]. Besides, the value of C_{12} in this work is 69.209 GPa, which is lower than the 75 GPa in both [79] and [80]. This suggests a reduced resistance to deformation along directions perpendicular to the crystal axis in this work. The value of C_{44} is consistent across all studies, with values of 43.58 GPa (this work), 43 GPa [83], and 43 GPa [82], indicating a similar resistance to shear deformation along the crystal planes.

3.2.2. Mechanical properties

The bulk modulus mentioned in this work from Table 2 is 248.10 GPa, close to 250 GPa [79] and 251 GPa [80], reflecting similar resistance to uniform compres-

sion across all studies. The shear modulus in this work is 88.37 GPa, slightly higher than 84 GPa in [79] and lower than 90 GPa in [80]. These variations are consistent with the differences in C_{11} and C_{12} between the studies. The Young's modulus in this work is 78.99 GPa, which is slightly higher than 75.53 GPa in [79] but lower than 80.39 GPa in [80]. These differences reflect the variations in the shear modulus and bulk modulus.

The results obtained in this work are generally consistent with previous studies, with minor variations observed in the elastic constants and mechanical properties. The slight discrepancies in values such as C_{11}, G, and E can be attributed to differences in computational methods or approximations used in the calculations, but these differences do not significantly impact the overall understanding of the material's mechanical behavior.

ZrO_2: The elastic constants and mechanical properties for ZrO_2 are compared across this work, [81], and [82]. In this work, the values of C_{11}, C_{12}, and C_{44} are 535, 97, and 51, respectively, resulting in a bulk modulus of 243.00 GPa, a shear modulus of 219.00 GPa, and a Young's modulus of 219.79 GPa. In [81], the values are 507, 99, and 63 for C_{11}, C_{12}, and C_{44}, respectively, leading to a bulk modulus of 235.00 GPa, a shear modulus of 204.00 GPa, and a Young's modulus of 234.18 GPa. In [82], the values of C_{11}, C_{12}, and C_{44} are much higher, with $C_{11} = 596, C_{12} = 137.04$, and $C_{44} = 74.34$, giving a bulk modulus of 290.134 GPa, a shear modulus of 136.464 GPa, and a Young's modulus of 545.12 GPa. These discrepancies suggest that the material in [82] is much stiffer, likely due to different computational techniques, material phases, or approximations used, whereas the results from this work and [81] indicate relatively lower stiffness value [82] presents higher values, with $C_{11} = 578.2$, $C_{12} = 120.9$, and $C_{44} = 82.6$, yielding a bulk modulus of 283.2 GPa, a shear modulus of 130 GPa, and a Young's modulus of 139.4 GPa for ZrO_2.

HfO_2: The elastic constants and mechanical properties for HfO_2 are compared between this work, [83], and [84]. In this work, the values C_{11}, C_{12}, and C_{44} are 564.08, 86.71, and 94.90, respectively, resulting in a bulk modulus of 245.83 GPa, a shear modulus of 127.27 GPa, and a Young's modulus of 102.24 GPa. [83] reports values of $C_{11} = 559$, $C_{12} = 93$, and $C_{44} = 69$, with corresponding mechanical properties of a bulk modulus of 248 GPa, a shear modulus of 115 GPa, and a Young's modulus of 99.6 GPa. [84] presents higher values, with $C_{11} = 578.2$, $C_{12} = 120.9$, and $C_{44} = 82.6$, yielding a bulk modulus of 283.2 GPa, a shear modulus [84] of 130 GPa, and a Young's modulus of 139.4 GPa.

The results indicate a relatively consistent trend in the elastic constants across the studies, with minor differences observed in C_{11} and C_{12}. This suggests that the material's stiffness is relatively stable, but with slight variations in its resistance to compression and shear between different computational approaches. The mechanical properties, particularly the bulk modulus, shear modulus, and Young's modulus, show more noticeable variations. [84] reports the highest values, indicating a material with greater overall stiffness compared to the results from this work and [83]. All values point toward HfO_2 being a relatively stiff and stable material, with subtle differences in stiffness depending on the specific computational framework.

CeO_2: The elastic constants and mechanical properties for CeO_2 are compared between this work, [85], and [86]. In this work, the values of C_{11}, C_{12}, and C_{44} are 335, 97, and 51, respectively, resulting in a bulk modulus of 176.33 GPa, a shear modulus of 119 GPa, and a Young's modulus of 248.24 GPa. Reference [85] reports $C_{11} = 371.83$, $C_{12} = 114.69$, and $C_{44} = 62.71$, yielding a bulk modulus of 200.40 GPa, a shear modulus of 128.57 GPa, and a Young's modulus of 252.88 GPa. Reference [86] presents values of $C_{11} = 354.79$, $C_{12} = 139.27$, and $C_{44} = 51.20$, resulting in a bulk modulus of 211.11 GPa, a shear modulus of 107.76 GPa, and a Young's modulus of 255.28 GPa.

The comparison reveals that the results from [85] and [86] generally show a higher stiffness in terms of bulk modulus, shear modulus, and Young's modulus than this work. The variations in C_{11}, C_{12}, and C_{44} between the studies point to different material behaviors, with [85] showing higher values for the elastic constants and mechanical properties, suggesting a slightly stiffer material. This is contrasted by the results from [86], which show a higher Young's modulus but lower shear modulus compared to [85]. Several elements could explain the variations between these three result sets: the choice of computational methodology, the selected approximation schemes, and the specific parameters employed in calculations. Despite these discrepancies, all three studies consistently indicate that CeO_2 exhibits relatively high stiffness, with small variations in the values of elastic constants and mechanical properties depending on the method and assumptions used.

For the comparison between these oxides, TiO_2 has a bulk modulus of 248.10 GPa, shear modulus of 88.37 GPa, and Young's modulus of 78.99 GPa, indicating moderate stiffness. ZrO_2 shows higher shear and Young's moduli (219.00 and 219.79 GPa, respectively) despite a slightly lower bulk modulus (243.00 GPa). This indicates better resistance to shear and tension in ZrO_2, which is stiffer overall than TiO_2.

For HfO_2, the bulk modulus is 245.83 GPa, the shear modulus is 127.27 GPa, and Young's modulus is 102.24 GPa. It is stiffer than TiO_2, especially in terms of shear resistance. CeO_2, however, shows the

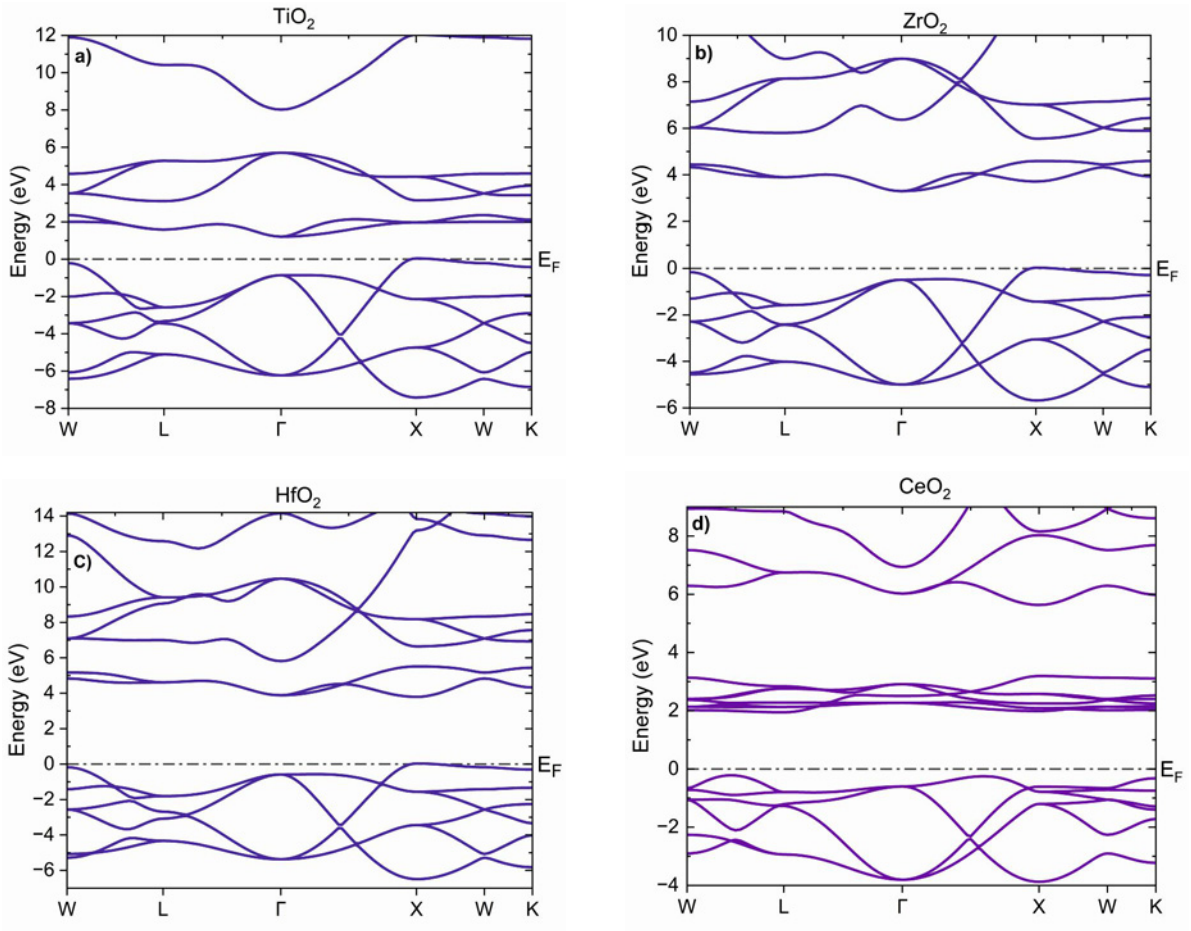

Fig. 2. Band structures of cubic dioxides: (a) c-TiO_2, (b) c-ZrO_2, (c) c-HfO_2, and (d) c-CeO_2, illustrating their distinctive electronic properties and band gap variations.

lowest bulk and shear moduli (176.33 and 119 GPa), though it has a relatively high Young's modulus of 248.24 GPa. This suggests CeO_2 is more compressible and shear-sensitive but retains good tensile stiffness.

3.3. Electronic properties

The electronic properties of materials are crucial for determining their functional applications in various fields. Therefore, Fig. 2 illustrates the band structures of the different c-XO_2 studied oxides. The band gap of TiO_2 is 1.15 eV, reflecting its semiconducting nature. This narrow gap allows visible-light absorption, making it suitable for photocatalysis but prone to carrier recombination. ZrO_2 has a wider band gap of 3.16 eV, indicative of its insulating behavior. Its strong ionic bonds result in high thermal and electrical stability. HfO_2 exhibits the largest band gap at 3.77 eV, reinforcing its status as an excellent insulator. This property, combined with low carrier mobility, makes it ideal for dielectric applications in microelectronics. CeO_2 has a moderate band gap of 2.17 eV, influenced by the mixed valence states of cerium. This feature enhances its redox properties and makes it effective for catalytic and oxygen storage applications. The band structures demonstrate significant differences in the electronic behaviors of these oxides, arising from variations in bonding strength and electronic interactions.

The (PDOS) illustrated in Fig. 3 for the various hybrides studied reveals distinct electronic structures and bonding characteristics. The partial density of states (PDOS) plots for TiO_2, ZrO_2, HfO_2, and CeO_2 provide valuable insights into their electronic structures and bonding characteristics, which are governed by the contributions of specific atomic orbitals. In ZrO_2, the valence band is dominated by O 2p orbitals, while the conduction band is primarily composed of Ti 3d orbitals, reflecting strong hybridization between O 2p and Ti 3d states. This hybridization results in a band gap of 1.15 eV, which is relatively narrow and supports TiO_2's semiconductor properties, making it suitable for applications in photocatalysis and optoelectronics. In ZrO_2, the valence band is similarly dominated by O 2p orbitals, but the conduction band is characterized by Zr 4d orbitals, leading to a wider band gap of 3.16 eV. This larger band gap and weaker hybridization compared to TiO_2 align with ZrO_2's insulating behavior and its use in high-k dielectrics and

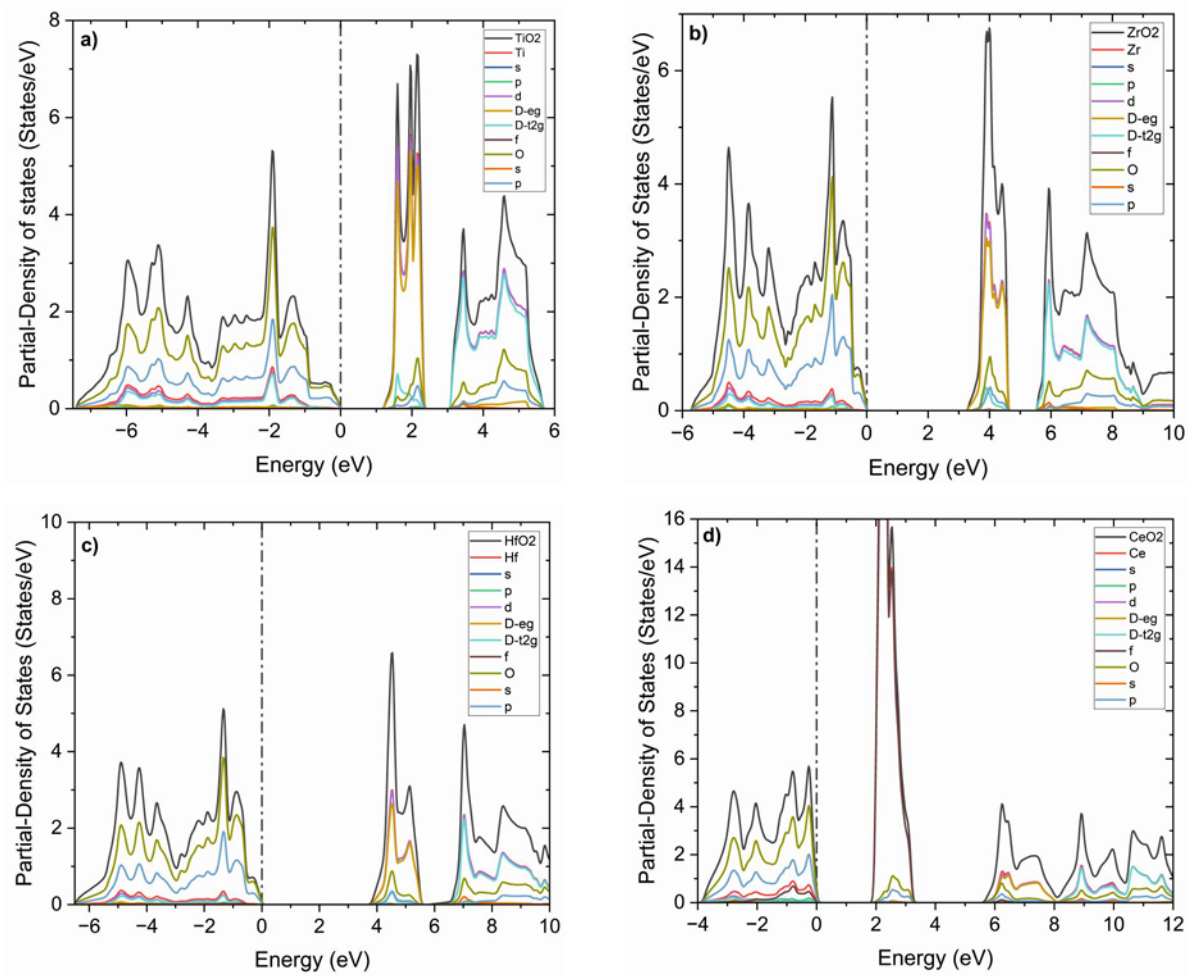

Fig. 3. Partial density of states (PDOS) for (a) c-TiO_2, (b) c-ZrO_2, (c) c-HfO_2, and (d) c-CeO_2, revealing their electronic structure and bonding characteristics.

thermal barrier coatings. HfO_2 exhibits a comparable trend, with O 2p orbitals dominating the valence band and Hf 5d orbitals shaping the conduction band, resulting in a band gap of 3.77 eV.

The slightly larger band gap and reduced hybridization in HfO_2 enhance its stability and suitability for advanced electronic applications, such as gate oxides in transistors. In contrast, CeO_2 displays a smaller band gap of 2.17 eV, attributed to the presence of Ce 4f states near the Fermi level, which introduces unique electronic properties such as redox activity and oxygen vacancy formation. The O 2p orbitals in all materials play a critical role in forming strong covalent bonds with the metal cations, while the metal d-orbitals (Ti 3d, Zr 4d, and Hf 5d) and f-orbitals (Ce 4f) determine the conduction band characteristics and influence the materials' optical, catalytic, and electronic properties.

4. Conclusions

In summary, we have performed ab initio modeling using the *Wien2k software* with the FP-LAPW method and the PBE exchange-correlation functional to investigate the structural, electronic, and mechanical properties of TiO_2, ZrO_2, HfO_2, and CeO_2. Our results show that the lattice parameters of TiO_2, ZrO_2, and CeO_2 increase with atomic mass, in line with the larger ionic radii of the metal cations. However, HfO_2 deviates from this trend, with a slightly smaller lattice parameter, likely due to stronger ionic bonding, which leads to a more compact crystal structure. This deviation underscores the complexity of the relationship between atomic size, bonding strength, and crystal packing in determining the structural properties of these oxides.

Regarding mechanical properties, ZrO_2 is the stiffest, demonstrating high resistance to shear and tension. HfO_2 follows, offering good shear resistance but lower overall stiffness. TiO_2 is moderately stiff, while CeO_2, the least stiff in compression and shear, shows strong tensile properties. These differences are directly related to variations in the crystal structures and atomic bonds of each oxide.

The electronic behavior of these oxides is reflected

in their band structures. TiO_2, with a narrow band gap of 1.15 eV, exhibits semiconductor properties, making it ideal for photocatalysis. ZrO_2 and HfO_2, with wider band gaps (3.16 and 3.77 eV), are better suited as insulators, while CeO_2, with a band gap of 2.17 eV, shows redox activity, making it valuable for catalytic processes. PDOS analysis indicates that O 2p orbitals dominate the valence bands, while metal d- and f-orbitals play a significant role in the conduction bands, influencing the oxides' performance in applications such as energy storage, catalysis, and electronics.

This work highlights that, despite these oxides sharing similar crystal structures and phases, significant differences in their characteristics emerge due to variations in the bonding and electronic configurations. This reinforces the importance of distinguishing between materials, even when they belong to the same group in the periodic table. The insights from this study deepen our understanding of these materials and provide a basis for selecting the most suitable oxide for specific applications. TiO_2, with its narrow band gap, excels in photocatalysis; ZrO_2 and HfO_2, with their insulating properties, are ideal for dielectric applications; and CeO2, with its redox activity, is promising for catalytic and energy storage applications. Future studies could further explore tuning these materials' properties through doping or phase transitions, expanding their utility in emerging technologies.

Acknowledgements

The authors acknowledge the use of institutional resources and facilities that supported the completion of this research.

References

[1] F. Zhang, S.-P. Yang, H.-M. Chen, X.-B. Yu, Preparation of discrete nanosize ceria powder, Ceram. Int. 30 (2004) 997–1002. https://doi.org/10.1016/j.ceramint.2003.10.018

[2] S. Park, J. M. Vohs, R. J. Gorte, Direct oxidation of hydrocarbons in a solid-oxide fuel cell, Nature 404 (2000) 265–267. https://doi.org/10.1038/35005040

[3] M. Maczka, E. T. G. Lutz, H. J. Verbeek, K. Oskam, A. Meijerink, J. Hanuza, M. Stuivinga, Spectroscopic studies of dynamically compacted monoclinic ZrO_2, Journal of Physics and Chemistry of Solids 60 (1999) 1909–1914. https://doi.org/10.1016/S0022-3697(99)00221-8

[4] M. Alvisi, M. Di Giulio, S. G. Marrone, M. R. Perrone, M. L. Protopapa, A. Valentini, L. Vasanelli, HfO_2 films with high laser damage threshold, Thin Solid Films 358 (2000) 250–258. https://doi.org/10.1016/S0040-6090(99)00690-2

[5] E. Bekyarova, P. Fornasiero, J. Kašpar, M. Graziani, CO oxidation on Pd/CeO_2-ZrO_2 catalysts, Catal. Today 45 (1998) 179–183. https://doi.org/10.1016/S0920-5861(98)00212-0

[6] A. Fujishima, T. N. Rao, D. A. Tryk, Titanium dioxide photocatalysis, Journal of Photochemistry and Photobiology C: Photochemistry Reviews 1 (2000) 1–21. https://doi.org/10.1016/S1389-5567(00)00002-2

[7] M. Grätzel, Photoelectrochemical cells, Nature 414 (2001) 338–344. https://doi.org/10.1038/35104607

[8] M. Adachi, I. Okada, S. Ngamsinlapasathian, Y. Murata, S. Yoshikawa, Dye-sensitized solar cells using semiconductor thin film composed of titania nanotubes, Electrochemistry 70 (2002) 449–452. https://doi.org/10.5796/electrochemistry.70.449

[9] M. Adachi, Y. Murata, M. Harada, S. Yoshikawa, Formation of titania nanotubes with high photocatalytic activity, Chem. Letters 29 (2000) 942–943. https://doi.org/10.1246/CL.2000.942

[10] K. Ishizaki, S. Komarneni, M. Nanko, Porous Materials: Process technology and applications, Springer New York, New York, 1998. https://doi.org/10.1007/978-1-4615-5811-8

[11] C. C. Wang, J. Y. Ying, Sol-gel synthesis and hydrothermal processing of anatase and rutile titania nanocrystals, Chemistry of Materials 11 (1999) 3113–3120. https://doi.org/10.1021/cm990180f

[12] N. Nehaoua, I. Ami, F. Mebtouche, H. Meziani, S. E. H. Abaidia, Performance analysis of organic-inorganic solar cell parameters evaluation from *I-V-G* curve: Numerical calculation, Romanian Journal of Physics 68 (2023) 608.

[13] R. Wang, K. Hashimoto, A. Fujishima, M. Chikuni, E. Kojima, A. Kitamura, M. Shimohigoshi, T. Watanabe, Light-induced amphiphilic surfaces, Nature 388 (1997) 431–432. https://doi.org/10.1038/41233

[14] J. Zhao, T. Wu, K. Wu, K. Oikawa, H. Hidaka, N. Serpone, Photoassisted degradation of dye pollutants. 3. Degradation of the cationic dye rhodamine b in aqueous anionic surfactant/TiO_2 dispersions under visible light irradiation: Evidence for the need of substrate adsorption on TiO_2 particles, Environ. Sci. Technol. 32 (1998) 2394–2400. https://doi.org/10.1021/ES9707926

[15] S. N. Frank, A. J. Bard, Heterogeneous photocatalytic oxidation of cyanide and sulfite in aqueous solutions at semiconductor powders, Journal of Physical Chemistry 81 (1977) 1484–1488. https://doi.org/10.1021/j100530a011

[16] S. N. Frank, A. J. Bard, Heterogeneous photocatalytic oxidation of cyanide ion in aqueous solutions at TiO_2 powder, J. Am. Chem. Soc. 99 (1977) 303–304. https://doi.org/10.1021/ja00443a081

[17] A. Fujishima, K. Honda, Electrochemical photolysis of water at a semiconductor electrode, Nature 238 (1972) 37–38. https://doi.org/10.1038/238037a0

[18] C. Su, C. M. Tseng, L. F. Chen, B. H. You, B. C. Hsu, S. S. Chen, Sol-hydrothermal preparation and photocatalysis of titanium dioxide, Thin Solid Films 498 (2006) 259–265. https://doi.org/10.1016/j.tsf.2005.07.123

[19] Y. Wang, Y. Huang, W. Ho, L. Zhang, Z. Zou, S. Lee, Biomolecule-controlled hydrothermal synthesis of C-N-S-tridoped TiO_2 nanocrystalline photocatalysts for NO removal under simulated solar light

irradiation, J. Hazard Mater. 169 (2009) 77–87. https://doi.org/10.1016/j.jhazmat.2009.03.071
[20] M. A. Fox, M. T. Dulay, Heterogeneous photocatalysis, Chem. Rev. 93 (1993) 341–357. https://doi.org/10.1021/cr00017A016
[21] M. R. Hoffmann, S. T. Martin, W. Choi, D. W. Bahnemann, Environmental applications of semiconductor photocatalysis, Chem. Rev. 95 (1995) 69–96. https://doi.org/10.1021/cr00033a004
[22] N. Nehaoua, I. Ami, F. Mebtouche, H. Meziani, S. H. Abaidia, Theoretical study of hybrid solar cell parameters evaluation from I-V characteristics, WSEAS Transactions on Circuits and Systems 21 (2022) 154–160. https://doi.org/10.37394/23201.2022.21.16
[23] Z. Shi, P. Yang, F. Tao, R. Zhou, New insight into the structure of CeO_2-TiO_2 mixed oxides and their excellent catalytic performances for 1,2-dichloroethane oxidation, Chemical Engineering Journal 295 (2016) 99–108. https://doi.org/10.1016/j.cej.2016.03.032
[24] N. Nolan, M. Seery, S. C. Pillai, Spectroscopic investigation of the anatase-to-rutile transformation of sol-gel-synthesized TiO_2 photocatalysts, Journal of Physical Chemistry C 113 (2009) 16151–16157. https://doi.org/10.1021/jp904358g
[25] J. Hidalgo-Jiménez, T. Akbay, Y. Ikeda, T. Ishihara, K. Edalati, Mechanism of anatase-to-columbite TiO_2 phase transformation via sheared phases: first-principles calculations and high-pressure torsion experiments, Journal of Materials Science 59 (2024) 5995–6007. https://doi.org/10.1007/s10853-023-09206-8
[26] S. Endo, H. Sato, J. Tang, Y. Nakamoto, T. Kikegawa, O. Shimomura, K. Kusaba, Baddeleyite-type high-pressure phase of TiO_2 and its stable *P-T* region. In: Y. Syono, M. H. Manghnani (Eds.), Geophysical Monograph Series, TERRAPUB, Tokyo, 1992. https://doi.org/10.1029/GM067p0457
[27] Y. Zhang, H. X. Chen, L. Duan, J. Bin Fan, L. Ni, V. Ji, A comparison study of the structural and mechanical properties of cubic, tetragonal, monoclinic, and three orthorhombic phases of ZrO_2, J. Alloys Compd. 749 (2018) 283–292. https://doi.org/10.1016/j.jallcom.2018.03.253
[28] T. Arima, S. Yamasaki, K. Yamahira, K. Idemitsu, Y. Inagaki, C. Degueldre, Evaluation of thermal conductivity of zirconia-based inert matrix fuel by molecular dynamics simulation, Journal of Nuclear Materials 352 (2006) 309–317. https://doi.org/10.1016/j.jnucmat.2006.02.066
[29] D. Simeone, G. Baldinozzi, D. Gosset, M. Dutheil, A. Bulou, T. Hansen, Monoclinic to tetragonal semireconstructive phase transition of zirconia, Phys. Rev. B Condens. Matter. Mater. Phys. 67 (2003) 064111. https://doi.org/10.1103/physrevb.67.064111
[30] J. Chevalier, S. Grandjean, M. Kuntz, G. Pezzotti, On the kinetics and impact of tetragonal to monoclinic transformation in an alumina/zirconia composite for arthroplasty applications, Biomaterials 30 (2009) 5279–5282. https://doi.org/10.1016/j.biomaterials.2009.06.022
[31] L. Gremillard, J. Chevalier, T. Epicier, S. Deville, G. Fantozzi, Modeling the aging kinetics of zirconia ceramics, J. Eur. Ceram. Soc. 24 (2004) 3483–3489. https://doi.org/10.1016/j.jeurceramsoc.2003.11.025
[32] X. Zhao, D. Vanderbilt, Phonons and lattice dielectric properties of zirconia, Phys. Rev. B Condens. Matter. Mater. Phys. 65 (2002) 1–10. https://doi.org/10.1103/physrevb.65.075105
[33] G. Stapper, M. Bernasconi, N. Nicoloso, M. Parrinello, Ab initio study of structural and electronic properties of yttria-stabilized cubic zirconia, Phys. Rev. B 59 (1999) 797–810. https://doi.org/10.1103/physrevb.59.797
[34] O. Ohtaka, H. Fukui, T. Kunisada, T. Fujisawa, K. Funakoshi, W. Utsumi, T. Irifune, K. Kuroda, T. Kikegawa, Phase relations and volume changes of hafnia under high pressure and high temperature, Journal of the American Ceramic Society 84 (2001) 1369–1373. https://doi.org/10.1111/J.1151-2916.2001.tb00843.x
[35] O. Ohtaka, H. Fukui, T. Kunisada, T. Fujisawa, K. Funakoshi, W. Utsumi, T. Irifune, K. Kuroda, T. Kikegawa, Phase relations and equations of state of ZrO_2 under high temperature and high pressure, Phys. Rev. B 63 (2001) 1741081–1741088. https://doi.org/10.1103/physrevb.63.174108
[36] S. Desgreniers, K. Lagarec, High-density ZrO_2 and HfO_2: Crystalline structures and equations of state, Phys. Rev. B 59 (1999) 8467–8472. https://doi.org/10.1103/physrevb.59.8467
[37] J. Haines, J. M. Léger, A. Atouf, Crystal structure and equation of state of cotunnite-type zirconia, Journal of the American Ceramic Society 78 (1995) 445–448. https://doi.org/10.1111/j.1151-2916.1995.tb08822.x
[38] J. M. Leger, P. E. Tomaszewski, A. Atouf, A. S. Pereira, Pressure-induced structural phase transitions in zirconia under high pressure, Phys. Rev. B 47 (1993) 14075–14083. https://doi.org/10.1103/physrevb.47.14075
[39] O. Ohtaka, H. Fukui, T. Kunisada, T. Fujisawa, K. Funakoshi, W. Utsumi, T. Irifune, K. Kuroda, T. Kikegawa, Phase relations and equations of state of ZrO_2 under high temperature and high pressure, Phys. Rev. B 63 (2001) 1741081–1741088. https://doi.org/10.1103/physrevb.63.174108
[40] J. Dewhurst, J. Lowther, Relative stability, structure, and elastic properties of several phases of pure zirconia, Phys. Rev. B 57 (1998) 741–747. https://doi.org/10.1103/PHYSREVB.57.741
[41] O. Ohtaka, T. Yamanaka, T. Yagi, New high-pressure and -temperature phase of ZrO_2 above 1000 °C at 20 GPa, Phys. Rev. B 49 (1994) 9295–9298. https://doi.org/10.1103/physrevb.49.9295
[42] A. Jayaraman, S. Y. Wang, S. K. Sharma, L. C. Ming, Pressure-induced phase transformations in HfO_2 to 50 GPa studied by Raman spectroscopy, Phys. Rev. B 48 (1993) 9205–9211. https://doi.org/10.1103/physrevb.48.9205
[43] O. Ohtaka, H. Fukui, T. Kunisada, T. Fujisawa, K. Funakoshi, W. Utsumi, T. Irifune, K. Kuroda, T. Kikegawa, Phase relations and equations of state of ZrO_2 under high temperature and high pressure, Phys. Rev. B 63 (2001) 1741081–1741088. https://doi.org/10.1103/physrevb.63.174108
[44] H. Arashi, T. Yagi, S. Akimoto, Y. Kudoh, New high-pressure phase of ZrO_2 above 35 GPa, Phys. Rev. B 41 (1990) 4309–4313. https://doi.org/10.1103/physrevb.41.4309

[45] M. Fadel, O. A. Azim M., O. Omer, R. R. Basily, A study of some optical properties of hafnium dioxide (HfO_2) thin films and their applications, Applied Physics A 66 (1998) 335–343. https://doi.org/10.1007/s003390050675
[46] M. Zukic, D. G. Torr, J. F. Spann, M. R. Torr, Vacuum ultraviolet thin films. 1: Optical constants of BaF_2, CaF_2, LaF_3, MgF_2, Al_2O_3, HfO_2, and SiO_2 thin films, Applied Optics 29 (1990) 4284–4292. https://doi.org/10.1364/AO.29.004284
[47] S. M. Edlou, A. Smajkiewicz, G. A. Al-Jumaily, Optical properties and environmental stability of oxide coatings deposited by reactive sputtering, Applied Optics 32 (1993) 5601–5605. https://doi.org/10.1364/AO.32.005601
[48] J. Khoshman, M. E. Kordesch, Optical properties of a-HfO_2 thin films, Surface and Coatings Technology 201 (2006) 3530–3535. https://doi.org/10.1016/j.surfcoat.2006.08.074
[49] J. Park, D. Lee, D. Lim, H. Lee, S.-H. Choi, Optical properties of thermally annealed hafnium oxide and their correlation with structural change, J. Appl. Phys. 104 (2008) 033521. https://doi.org/10.1063/1.2961326
[50] A. P. Menushenkov, D. S. Leshchev, A. A. Yaroslavtsev, V. V. Popov, J. Bednarcik, R. V. Chernikov, Crystal structure of [Dy_2O_3]:[HfO_2] oxides: Combined synchrotron study.
[51] Y. Qi, S. Singh, C. Lau, F. T. Huang, X. Xu, F. J. Walker, C. H. Ahn, S. W. Cheong, K. M. Rabe, Stabilization of competing ferroelectric phases of HfO_2 under epitaxial strain, Phys. Rev. Lett. 125 (2020) 257603. https://doi.org/10.1103/physrevlett.125.257603
[52] W. Lee, T. Katoh, H. Kang, J. Park, U. G. Paik, H. T. Jeon, Effects of abrasive size and surfactant in nano ceria slurry for shallow trench isolation, Journal of the Korean Physical Society 44 (2004) L796-L799.
[53] Y. Gu, C. Gu, Y. Zhang, Z. Mu, X. Liu, Mastering lanthanide energy states for next-gen photonic innovation, Science China Chemistry 66 (2023) 2460–2479. https://doi.org/10.1007/s11426-023-1609-y
[54] A. Trovarelli, Catalysis by Ceria and Related Materials, Imperial College Press, London, 2002. https://doi.org/10.1142/p249
[55] H. Inaba, H. Tagawa, Ceria-based solid electrolytes, Solid State Ionics 83 (1996) 1–12. https://doi.org/10.1016/0167-2738(95)00229-4
[56] A. Kossoy, Q. Wang, R. Korobko, V. Grover, Y. Feldman, E. Wachtel, A. K. Tyagi, A. I. Frenkel, I. Lubomirsky, Evolution of the local structure at the phase transition in CeO_2-Gd_2O_3 solid solutions, Phys. Rev. B 87 (2013) 054101. https://doi.org/10.1103/physrevb.87.054101
[57] M. Morishita, T. Kakeya, M. Kanemoto, M. Kodama, T. Sakai, Improvement of stability at low potential and structure of cobalt oxyhydroxide/CeO_2 composite as additive for nickel hydroxide electrode, J. Electrochem. Soc. 159 (2012) A2069–A2075. https://doi.org/10.1149/2.072212jes
[58] T. V. Ivanova, J. Toivonen, P. S. Maydannik, T. Kääriäinen, M. Sillanpää, T. Homola, D. C. Cameron, Atomic layer deposition of cerium oxide for potential use in diesel soot combustion, J. Vac. Sci. Technol. A 34 (2016) 031506. https://doi.org/10.1116/1.4944589
[59] X. Liu, K. Zhou, L. Wang, B. Wang, Y. Li, Oxygen vacancy clusters promoting reducibility and activity of ceria nanorods, J. Am. Chem. Soc. 131 (2009) 3140–3141. https://doi.org/10.1021/ja808433d
[60] S. S. Mofarah, E. Adabifiroozjaei, Y. Yao, P. Koshy, S. Lim, R. Webster, X. Liu, R. Khayyam Nekouei, C. Cazorla, Z. Liu, Y. Wang, N. Lambropoulos, C. C. Sorrell, Proton-assisted creation of controllable volumetric oxygen vacancies in ultrathin CeO_{2-x} for pseudocapacitive energy storage applications, Nature Comm. 10 (2019) 2594. https://doi.org/10.1038/s41467-019-10621-2
[61] S. Pavasupree, Y. Suzuki, S. Pivsa-Art, S. Yoshikawa, Preparation and characterization of mesoporous MO_2 (M = Ti, Ce, Zr, and Hf) nanopowders by a modified sol-gel method, Ceramics International 31 (2005) 959–963. https://doi.org/10.1016/j.ceramint.2004.10.009
[62] T. I. Panova, V. P. Popov, V. B. Glushkova, A. V. Domanskii, Preparation of nanodisperse solid solutions based on ZrO_2 and HfO_2 from hydroperoxides, Glass Physics and Chemistry 33 (2007) 652–657. https://doi.org/10.1134/s108765960706017x
[63] Y. Yang, X. Fan, C. Liu, R. X. Ran, First principles study of structural and electronic properties of cubic phase of ZrO_2 and HfO_2, Physica B: Condensed Matter 434 (2014) 7–13. https://doi.org/10.48550/arXiv.cond-mat/0301016
[64] G.-M. Rignanese, IVb Transition metal oxides and silicates: An ab initio study, Materials Fundamentals of Gate Dielectrics (2006) 249–290. https://doi.org/10.1007/1-4020-3078-9_7
[65] L. Zibordi-Besse, Y. Seminovski, I. Rosalino, D. Guedes-Sobrinho, J. L. F. Da Silva, Physical and chemical properties of unsupported $(MO_2)n$ clusters for M = Ti, Zr, or Ce and n = 1–15: A density functional theory study combined with the tree-growth scheme and Euclidean similarity distance algorithm, Journal of Physical Chemistry C 122 (2018) 27702–27712. https://doi.org/10.1021/acs.jpcc.8b08299
[66] W. Kohn, L. J. Sham, Self-consistent equations including exchange and correlation effects, Physical Review 140 (1965) A1133. https://doi.org/10.1103/physrev.140.A1133
[67] P. Blaha, K. Schwarz, G. K. H. Madsen, D. Kvasnicka, J. Luitz, R. Laskowski, F. Tran, L. D. Marks, WIEN2k: An Augmented Plane Wave Plus Local Orbitals Program for Calculating Crystal Properties, Abstract: User's Guide, WIEN2k 19.1. Techn. Universitat 2019. ISBN: 3-950103112
[68] J. L. Erskine, E. A. Stern, Magneto-optic Kerr effect in Ni, Co, and Fe, Phys. Rev. Lett. 30 (1973) 1329–1332. https://doi.org/10.1103/physrevlett.30.1329
[69] A. Petukhov, I. Mazin, L. Chioncel, A. I. Lichtenstein, Correlated metals and the LDA + U method, Physical Review B 67 (2003) 153106. https://doi.org/10.1103/PhysRevB.67.153106
[70] J. P. Perdew, K. Burke, M. Ernzerhof: Perdew, Burke, and Ernzerhof Reply, Phys. Rev. Lett. 80 (1998) 891. https://doi.org/10.1103/physrevlett.80.891
[71] P. Novák, J. Kuneš, L. Chaput, W. E. Pickett, Exact exchange for correlated electrons, Phys. Status Solidi B Basic Res. 243 (2006) 563–572. https://doi.org/10.1002/pssb.200541371

[72] F. Birch, Finite elastic strain of cubic crystals, Physical Review 71 (1947) 809–824. https://doi.org/10.1103/PhysRev.71.809
[73] M. Abbasnejad, E. Shojaee, M. R. Mohammadizadeh, M. Alaei, R. Maezono, Quantum Monte Carlo study of high-pressure cubic TiO_2, Appl. Phys. Lett. 100 (2012) 261902. https://doi.org/10.1063/1.4730608
[74] M. Mattesini, J. S. De Almeida, L. Dubrovinsky, N. Dubrovinskaia, B. Johansson, R. Ahuja, High-pressure and high-temperature synthesis of the cubic TiO_2 polymorph, Phys. Rev. B 70 (2004) 212101. https://doi.org/10.1103/PhysRevB.70.212101
[75] Z. W. Niu, B. Zhu, Y. Cheng, R. N. Song, G. F. Ji, Elastic and electronic properties of cubic cerium oxide under pressure via first principles, Int. J. Mod. Phys. B 28 (2014) 1450070. https://doi.org/10.1142/S0217979214500702
[76] J. Wang, H. P. Li, R. Stevens, Hafnia and hafnia-toughened ceramics, Journal of Materials Science 27 (1992) 5397–5430. https://doi.org/10.1007/BF00541601
[77] K. Clausen, W. Hayes, J. E. Macdonald, R. Osborn, P. G. Schnabel, M. T. Hutchings, A. Magerl, Inelastic neutron scattering investigation of the lattice dynamics of ThO_2 and CeO_2, Journal of the Chemical Society, Faraday Transactions 2: Molecular and Chemical Physics 83 (1987) 1109–1112. https://doi.org/10.1039/F29878301109
[78] A. Bouhemadou, Theoretical study of the structural, elastic and electronic properties of the GeX_2O_4 (X= Mg, Zn, Cd) compounds under pressure, Modelling Simul. Mater. Sci. Eng. 16 (2008) 055007. http://dx.doi.org/10.1088/0965-0393/16/5/055007
[79] M. De Jong, W. Chen, T. Angsten, A. Jain, R. Notestine, A. Gamst, M. Sluiter, C. K. Ande, S. Van Der Zwaag, J. J. Plata, C. Toher, S. Curtarolo, G. Ceder, K. A. Persson, M. Asta, Charting the complete elastic properties of inorganic crystalline compounds, Dryad Digital Repository 2 (2015) 150009. https://doi.org/10.1038/sdata.2015.9
[80] F. Semari, T. Ouahrani, H. Khachai, R. Khenata, M. Rabah, A. Bouhemadou, G. Murtaza, B. Amin, D. Rached, Electronic band structure, optical, thermal and bonding properties of XMg_2O_4 (X = Si, Ge) spinel compounds, Int. J. Mod. Phys. B 27 (2013). https://doi.org/10.1142/S0217979213500823
[81] I. Najdhefer, A. Kapidžić, Ab-initio calculations of cubic and tetragonal ZrO_2 doped with Cd, Y, Y+Nb, Y+Ta-charge-compensating dopants: Structural and electrostatic calculations, Radiation Physics and Chemistry 222 (2024) 111804. https://doi.org/10.1016/j.radphyschem.2024.111804
[82] I. D. Muhammad, M. Awang, O. Mamat, Z. Bt Shaari, First-principles calculations of the structural, mechanical and thermodynamics properties of cubic zirconia, World Journal of Nano Science and Engineering 4 (2014) 97–103. http://dx.doi.org/10.4236/wjnse.2014.42013
[83] C. A. Ponce, R. A. Casali, M. A. Caravaca, Ab initio study of mechanical and thermo-acoustic properties of tough ceramics: applications to HfO_2 in its cubic and orthorhombic phase, Journal of Physics: Condensed Matter 20 (2008) 045213. https://doi.org/10.1088/0953-8984/20/04/045213
[84] S. L. Dole, O. Hunter, C. J. Wooge, Elastic properties of monoclinic hafnium oxide at room temperature, Journal of the American Ceramic Society 60 (1977) 488–490. https://doi.org/10.1111/J.1151-2916.1977.TB14088.X
[85] S. Shi, X. Ke, C. Ouyang, H. Zhang, H. Ding, Y. Tang, W. Zhou, P. Li, M. Lei, W. Tang, First-principles investigation of the bonding, optical and lattice dynamical properties of CeO_2, J. Power Sources 194 (2009) 830–834. https://doi.org/10.1016/J.JPOWSOUR.2009.06.031
[86] J. Buckeridge, D. Scanlon, A. Walsh, A. A. Sokol, Dynamical response and instability in ceria under lattice expansion, Phys. Rev. B 87 (2013) 214304. https://doi.org/10.1103/physrevb.87.214304
[87] Y. Yang, X. Fan, C. Liu, R. X. Ran, First principles study of structural and electronic properties of cubic phase of ZrO_2 and HfO_2, Physica B: Condensed Matter 434 (2014) 7–14. https://doi.org/10.1016/j.physb.2013.10.037
[88] N. Igawa, Y. Ishii, T. Nagasaki, Y. Morii, S. Funahashi, H. Ohno, Crystal structure of metastable tetragonal zirconia by neutron powder diffraction study, Journal of the American Ceramic Society 76 (1993) 2673–2676. https://doi.org/10.1111/J.1151-2916.1993.TB03999.X